ELSEVIER

Cellular pattern formation during retinal regeneration: A role for homotypic control of cell fate acquisition

Melinda J. Tyler [a,b], David A. Cameron [a,*]

[a] *Department of Neuroscience and Physiology, SUNY Upstate Medical University, 750 E. Adams St., Syracuse, NY 13210, USA*
[b] *MD/PhD Program, SUNY Upstate Medical University, Syracuse, NY, USA*

Abstract

A dominant mechanism of cellular patterning in the growing fish retina is control of cell fate acquisition by negative feedback signals arising from differentiated cells. We tested the ability of a computational model of this pattern formation mechanism to simulate cellular patterns in regenerated goldfish retina. The model successfully simulated quantitative features of *in vivo* regenerated patterns, indicating that regenerating retina has access to and utilizes patterning mechanisms that are operational during normal growth. The atypical patterns of regenerated retina could arise in part from regenerative progenitors that, compared to normal growth progenitors, are less responsive to the feedback patterning signals.
© 2006 Elsevier Ltd. All rights reserved.

1. Introduction

The lack of neuronal regeneration in the human central nervous system is a contributing factor to the functional deficits often associated with neurological disease and trauma. In contrast, the central nervous systems of fish and amphibians exhibit a capacity for substantial cellular regeneration. Much experimental attention has been focused upon regeneration of the anamniote retina, with evidence mounting that the underlying mechanisms resemble those of development (Cameron, Gentile, Middleton, & Yurco, 2005; Cheon, Kuwata, & Saito, 2001; Chiba, Nakamura, Unno, & Saito, 2004; Chiba, Oi, & Saito, 2005; Goldman, Hankin, Li, Dai, & Ding, 2001; Mader & Cameron, 2004; Naruoka, Kojima, Ohmasa, Layer, & Saito, 2003; Ohmasa & Saito, 2004; Otteson & Hitchcock, 2003; Raymond & Hitchcock, 2000; Reh & Levine, 1998; Saito, Kaneko, Maruo, Niino, & Sakaki, 1994; Stenkamp & Cameron, 2002). Many key aspects of regenerative cytogenesis

in the retina, however, such as the molecular determinants of cell fate acquisition, remain unresolved. By extension it is not clear why atypical cellular patterns, which may negatively impact functional recovery, emerge in regenerated retina (Braisted, Essman, & Raymond, 1994; Cameron & Carney, 2000; Cameron & Easter, 1995; Hitchcock & VanDeRyt, 1994).

With respect to defining the mechanisms that control cellular pattern formation in the growing retina, computational modeling provides a powerful method for generating testable hypotheses. Several studies have used computational approaches to investigate and objectively evaluate candidate patterning mechanisms during normal retinal development such as the control of cell migration and/or differentiation (Cameron & Carney, 2004; Eglen, van Ooyen, & Willshaw, 2000; Eglen & Willshaw, 2002; Raven, Eglen, Ohab, & Reese, 2003; Tohya, Mochizuki, & Iwasa, 1999, 2003; Tyler, Carney, & Cameron, 2005). Computational models of cellular pattern formation during retinal regeneration, however, are absent. There is thus a limited theoretical basis for predicting whether regenerative patterning mechanisms are similar

---

* Corresponding author. Fax: +1 315 464 7712.
  E-mail address: camerond@upstate.edu (D.A. Cameron).

to, or significantly different from, those in operation during normal retinal growth.

The aims of the current investigation were to evaluate a dynamic computational model of cellular pattern formation during retinal regeneration and to identify modeled parameters that could account quantitatively for the atypical cellular patterns observed within the regenerated structure. Previous empirical and computational analyses have indicated that, in the inner retina of fish, cellular pattern formation is dominated by mechanisms through which cell fate decisions are controlled via a set of independent, homotypic, inhibitory signals arising from differentiated cells (Cameron & Carney, 2004; Tyler et al., 2005). To determine if similar mechanisms might control cellular patterning during adult retinal regeneration, we empirically evaluated regenerated goldfish retina and performed computational simulations of regenerative growth. The results suggest that, as with normal retinal growth, cellular pattern formation in regenerating retina is dominated by inhibitory, or negative feedback, signals that control cell fate acquisition in a homotypic manner, indicating a regenerative recapitulation of developmental patterning mechanisms. Evidence is also provided that suggests the atypical cellular patterns of regenerated retina might emerge as a consequence of both geometric characteristics of the regenerating structure and regenerative progenitors with lower sensitivity to the feedback signals than that inferred for normal growth progenitors.

2. Methods

2.1. Model system, intraocular drug delivery, and surgical lesion

Adult, light-adapted goldfish (*Carassius auratus*) of standard length 4.8–7.5 cm (mean 5.7 ± 0.7, $n = 34$) were used for all experiments. Animal use was approved by the Committee for the Humane Use of Animals, SUNY Upstate Medical University. To control for cellular pattern attributes that might vary as a function of fish size or retinal hemifield, fish of similar standard lengths were used and cellular patterns were analyzed only for dorsal retina. The procedures and details of intraocular application of the neurotoxin 6-hydroxydopamine (6-OHDA) or vehicle only (Tyler et al., 2005), and surgical excision of a patch of dorsal retina from one eye of each fish (Cameron & Easter, 1995; Hitchcock, Lindsey Myhr, Easter, Mangione-Smith, & Jones, 1992) were as described previously. 6-OHDA selectively ablates retinal tyrosine hydroxylase-positive cells (TH+), the putative dopaminergic neurons of the goldfish retina. Following surgery, fish were returned to their tanks and maintained for at least 12 weeks.

2.2. Immunohistochemistry

Detection of TH+ and serotonin-positive (5-HT+) cells was achieved in retinal whole mounts using procedures described previously (Cameron & Carney, 2000, 2004; Tyler et al., 2005). These two inner nuclear layer neuron subtypes were chosen for pattern analysis due to the ease of selective labeling and neurotoxin-mediated ablation, as well as the previously characterized regularity of their two-dimensional patterns (Cameron & Carney, 2000, 2004; Tyler et al., 2005). Briefly, light-adapted retinas were fixed (0.25% picric acid/4% paraformaldehyde/0.1 M PO₄, pH 7.0), flat mounted, and processed for indirect epifluorescence immunohistochemical labeling of TH+ or 5-HT+ cells. The primary antibodies used were anti-TH (Cat. #MAB318; Chemicon, Temecula, CA) and/or anti-5-HT (Cat. #MAB352;

Chemicon, Temecula, CA). Secondary antibodies (Cy3- or Cy2-conjugated; Jackson ImmunoResearch, West Grove, PA) were used to screen for primary antibody labeling; to enhance detection of 5-HT+ cells a tertiary antibody with the same conjugated fluorophore as the secondary antibody was often utilized. The reacted tissue was washed repeatedly with phosphate-buffered saline, mounted on a glass slide (pigmented epithelium side down), and visualized with standard epifluorescence light microscopy. The location and boundary determination of patches of regenerated retina were achieved by (a) identification of dorsal hemiretina via ocular landmarks and (b) evaluation and mapping of discontinuities in the cone mosaic structure between extant and regenerated retina (Braisted et al., 1994; Cameron & Easter, 1995). Fields of labeled cells of area approximately 0.5 mm² were collected with a digital image capture system (Metamorph).

2.3. Quantitative analysis of cellular patterns

The two-dimensional patterns of TH+ and 5-HT+ cells were analyzed using spatial pattern analyses described previously (Cameron & Carney, 2000, 2004; Tyler et al., 2005). Briefly, for a given field of labeled cells in control or regenerated retina (two non-overlapping fields were sampled from each retina) each labeled soma was assigned a two-dimensional Cartesian coordinate value. For each field the set of coordinate values was evaluated quantitatively using three analyses: nearest neighbor distance (NND), density recovery profile (DRP), and quadrat analyses. The attributes and application of each analysis have been described in depth (Greig-Smith, 1957; Rodieck, 1991; Cook, 1996; Cameron & Carney, 2000, 2004; Eglen et al., 2000; Stenkamp, Powers, Carney, & Cameron, 2001). All cell density measurements and pattern analyses were performed using custom software (Tyler et al., 2005).

2.4. Computational modeling of retinal cell pattern formation

A computational, dynamic model of cellular pattern formation was tested for its ability to simulate the cellular organization and assembly of regenerated retina. The fundamental details of this model have been described previously (Cameron & Carney, 2004; Tyler et al., 2005). Briefly, the model utilizes a physiologically realistic, negative feedback signaling mechanism that controls cell fate acquisition within an undifferentiated neuroepithelium. In the model, cell fates are regulated by signals that inhibit the production of homotypic cells. These signals originate from each differentiated cell and decay exponentially with distance. The space constant describing the exponential decay determines the density of newly produced cells. This model successfully recapitulates cell pattern formation in the inner retina during normal growth of the goldfish retina; other hypothetical patterning mechanisms, such as migration of differentiated cells, are not required. Additionally, the computational model accurately simulates cellular pattern formation in growing retina subsequent to selective ablation of differentiated retinal neurons (Tyler et al., 2005).

For this report the computational model was extended to mimic regenerative growth of the goldfish retina after surgical lesion. Specifically, model-derived growth was altered so that cellular assembly proceeded from the edge of a lesion site into the region of excised retina, matching a commonly accepted geometry of retinal lesion resolution in adult fish (Hitchcock et al., 1992; Yurco & Cameron, 2005). To accommodate and evaluate the complex geometries of this "inward" regenerative growth, three geometric lesion conditions were tested: a circular patch, a square patch, and a roughly square patch with jagged edges. The latter geometry is hypothesized to best represent the spatial contours of surgically excised retina, whereas the former two conditions provide well defined, idealized geometric conditions that are relatively easily implemented.

For each model simulation of regenerative growth of TH+ patterns (six simulations were run for each geometric condition) a virtual control retina was first derived from simulated normal growth, using the "seed" coordinates of labeled cells derived from actual goldfish retina (Tyler et al., 2005). These model-derived control patterns were not significantly different from the actual *in vivo* patterns (see Section 3), but provided larger areas from which to collect quantitative pattern information. Within the central

region of the large model-derived pattern a circular, square, or jagged region of minimum total area 4.0 mm² was removed. A 50 μm wide band of randomly patterned undifferentiated cells was then affixed contiguously to the excision boundary, consisting of a cellular density previously demonstrated to be sufficient for simulating the patterns of inner retinal cells (based on estimates from empirical measurements of the circumferential germinal zone; Cameron & Carney, 2004; Tyler et al., 2005). Increasing the density of these cells did not affect the results nor did decreases to the lowest tested value of 50% (data not shown).

Modeled regenerative growth was initiated using cell-type-specific parameters appropriate for normal retinal growth (Cameron & Carney, 2004; Tyler et al., 2005). In later simulations the parameter representing the threshold of undifferentiated cells to the inhibitory signal was varied in an effort to improve the match between the cell density of the *in vivo* and model-derived regenerated cell patterns (see Section 3; Fig. 8 of Cameron & Carney, 2004). Following each iteration of regenerative growth (i.e., 50 μm linear growth into the lesion site) a new band of randomly distributed undifferentiated cells was generated and affixed to the new lesion edge, and the feedback signal profile determined *de novo*. Regenerative growth continued in this manner until the excision site was filled with regenerated cells. As with the earlier modeling of normal retinal growth the feedback signal is assumed to not accumulate (sum) across iterations. To evaluate patterning in the simulated regenerated retina a region of fixed area completely within the final, model-derived regenerated pattern was analyzed with NND, DRP, and quadrat analysis. For each simulation the area of analyzed retina (0.5 mm²) approximated that analyzed for

in vivo retinas. Copies of the model code (in MatLab) are available from the corresponding author.

3. Results

3.1. Cellular patterns in control and regenerated goldfish retina

Quantitative, two-dimensional spatial pattern analyses of TH⁺ cells in six control retinas were performed. The results are summarized in Table 1. Autocorrelation NND (aNND) analysis revealed normal distributions with values 92.3 ± 9.1 μm (mean ± SD; $n = 12$ non-overlapping samples). Conformity ratio (CR) analysis of the aNND distributions indicated that the patterns were significantly different ($p < .05$) from those expected for a random distribution (CR value 3.9 ± 0.6, $n = 12$; Cook, 1996). Autocorrelation DRP (aDRP) analysis revealed effective radius values (Rodieck, 1991) of 76.5 ± 13.5 μm ($n = 12$), indicating the presence of local anti-clustering. Quadrat analysis indicated pattern regularity over large spatial scales. These analyses revealed that patterns of TH⁺ cells in control

Table 1
Spatial analyses of *in vivo* control and regenerated TH⁺ cell patterns

ID (n)	NND (μm) mean ± SD	CR	Density (mm⁻²)	R_{eff} (μm)	Quadrat
Control					
TH1a (38)	86.3 ± 25.5	3.4	75.4	66	Regular
TH1b (41)	74.3 ± 20.7	3.6	81.3	45	Regular
TH2a (38)	87.1 ± 23.1	3.8	75.4	77	Regular
TH2b (41)	79.9 ± 21.6	3.7	81.3	68	Regular
TH3a (33)	98.2 ± 24.7	4.0	65.5	82	Regular
TH3b (42)	89.8 ± 22.2	4.0	83.3	87	Regular
TH4a (29)	99.4 ± 27.7	3.6	57.5	99	Regular
TH4b (30)	106.2 ± 21.2	5.0	59.5	85	Regular
TH5a (28)	94.9 ± 20.1	4.7	55.6	69	Regular
TH5b (27)	99.6 ± 32.3	3.1	53.6	78	Regular
TH6a (35)	95.4 ± 20.8	4.6	69.4	79	Regular
TH6b (30)	96.6 ± 29.6	3.6	59.5	83	Regular
Mean ± SD	92.3 ± 9.1	3.9 ± 0.6	68.1 ± 11.0	76.5 ± 13.5	
p values					
Regenerated					
TH1a (45)	71.4 ± 28.6	2.5	89.3	47	Reg/rand
TH1b (38)	60.6 ± 24.3	2.5	75.4	0	Random
TH2a (49)	68.8 ± 23.1	3.0	97.2	48	Reg/rand
TH2b (45)	71.0 ± 33.7	2.1	89.3	52	Reg/rand
TH3a (52)	65.7 ± 23.5	2.8	103.2	53	Reg/rand
TH3b (53)	64.6 ± 24.2	2.7	105.2	85	Reg/rand
TH4a (50)	68.9 ± 22.2	3.1	99.2	62	Regular
TH4b (75)	47.8 ± 31.1	1.5	148.8	30	Random
TH5a (29)	55.8 ± 33.5	1.7	57.5	12	Clust/rand
TH5b (59)	52.8 ± 32.4	1.6	117.1	0	Random
TH6a (40)	78.4 ± 22.3	3.5	79.4	69	Regular
TH6b (42)	76.9 ± 29.5	2.6	83.3	59	Reg/rand
Mean ± SD	65.2 ± 9.4	2.5 ± 0.6	95.4 ± 23.0	43.1 ± 27.1	
p values	<.001	<.001	<.005	<.001	

For each sampled retina in each category two non-overlapping regions were analyzed. The result of statistical comparison between the control and regenerated data is reported as the *p* value from independent *t*-test analysis. ID, sampled region identifier; *n*, number of analyzed cells; NND, nearest neighbor distance; CR, conformity ratio (Cook, 1996); R_{eff}, effective radius (Rodieck, 1991); Quadrat, pattern attributes derived from the dispersion index function of quadrat analysis (Stenkamp et al., 2001) recorded as regular, random, Reg/rand (dispersion index distributed equally between regular and random), or Clust/rand (dispersion index values distributed equally between clustered and random).

retina are non-random, consistent with an earlier report (Tyler et al., 2005).

Visual inspection of lesioned retinas 12 weeks following surgery revealed successful retinal regeneration, as indicated by a localized region in dorsal retina of substantial disruption in the cone mosaic (Fig. 1A; Cameron & Easter, 1995). TH^{+} cells were present in regenerated retina (Fig. 1B), but aberrations in their cellular patterns were evident; summary information for individual data sets from regenerated retinas is tabulated in Table 1. Consistent with earlier reports (Cameron & Carney, 2000; Hitchcock & VanDeRyt, 1994) the density of regenerated TH^{+} cells was significantly elevated compared to control retinas (Fig. 2D, independent *t*-test $p < .001$). For regenerated TH^{+} cells the aNND values were significantly smaller than in control retinas, as expected for a higher density of cells (Fig. 2A, $65.2 \pm 9.4 \,\mu m$, $n = 12$; $p < .001$). CR analysis indicated that regenerated patterns, although non-random, were significantly less regular than those of control retinas (Fig. 2B, conformity ratio $2.5 \pm .6$, $n = 12$; $p < .001$). DRP analysis revealed regenerated effective radius values that were significantly lower than controls, suggesting a disruption in homotypic anti-clustering during regeneration (Fig. 2C, $43.1 \pm 27.1 \,\mu m$, $n = 12$; $p < .001$). Lastly, quadrat analysis

Fig. 2. Spatial analysis of control and regenerated TH[+] cell patterns *in vivo*. Nearest neighbor distance (NND; A), conformity ratio (B), effective radius (C), and cell density (D) analyses all revealed consistent, statistically significant differences in the patterns of TH^{+} cells in control and regenerated retina (cf. Table 1). Values presented as means ± standard deviation.

revealed that regenerated patterns tended to be less regular than those of control retina (Table 1). These analyses indicated that although TH^{+} cells were present in regenerated retinas, they were arrayed in two-dimensional patterns significantly different from, and disrupted relative to, the patterns of control retinas.

3.2. Effects of targeted cell ablation upon regenerated cellular patterns

To investigate the determinants of cellular pattern formation in regenerated retina, patterns of TH[+] and 5-HT^{+} cells were analyzed in retinas exposed to 6-OHDA prior to surgical lesion. By utilizing a neurotoxin specific for only one of the neuron types but examining patterns of both cell types, it was possible to rule out heterotypic effects upon pattern formation of neurons residing within the same retinal lamina, confirming findings of previous studies involving goldfish and zebrafish retinal growth (Cameron & Carney, 2000, 2004; Tyler et al., 2005). Neurotoxin specificity was confirmed by the loss of TH[+] but not 5-HT^{+} cells, consistent with earlier reports (Fig. 3; Negishi, Teranishi, & Kato, 1982; Watling, Parkinson, & Dowling, 1982; Reh & Tully, 1986; Yazulla & Studholme, 1997; Tyler et al., 2005). TH^{+} cells were present in regenerated retina but not in the extant, neurotoxin exposed retina, indicating a lack of lateral migration of regenerated TH^{+} cells into the denuded retina (Fig. 3A). Furthermore, a significantly elevated density of regenerated TH^{+} cells, on the order of 1.7-fold compared to control, was observed adjacent to the original
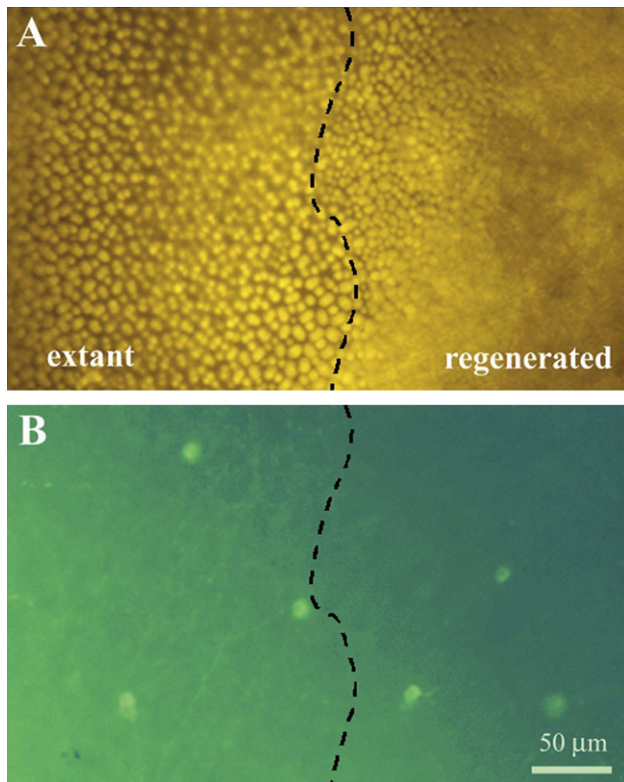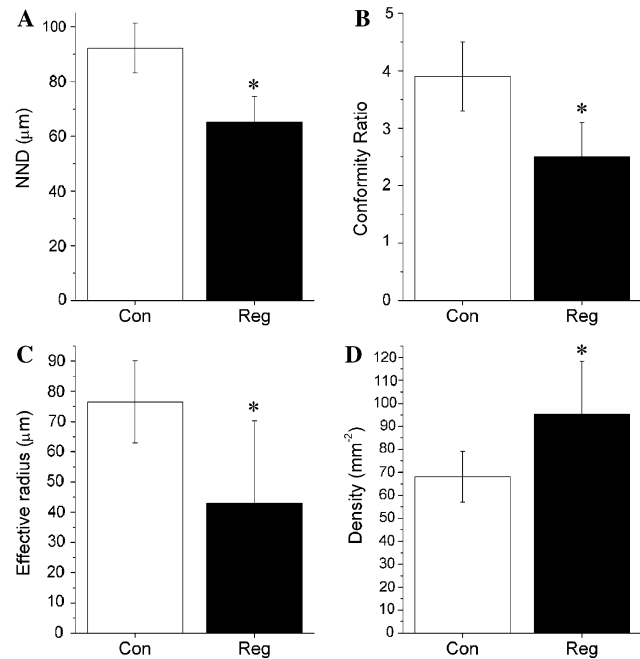

Fig. 1. Identification of regenerated retina *in vivo*. (A) Cone photoreceptors viewed in a retinal whole-mount. The cone mosaic of regenerated retina (right of the dotted line) is overtly disrupted relative to the adjoining extant retina (left of the dotted line). (B) TH^{+} cells viewed in the same retinal whole-mount as (A), with the focal plane adjusted to the inner retina. The TH^{+} cells in the regenerated region tend to be packed more closely than those in extant retina, suggesting a disruption in TH[+] cell patterning (see Section 3 and Table 1).
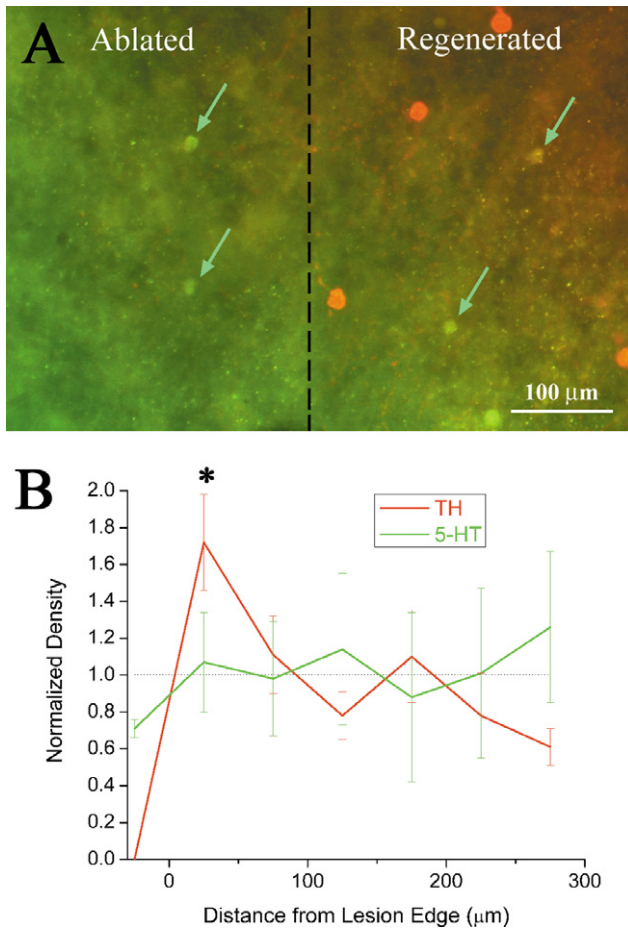
Fig. 3. Regeneration of TH$^+$ cells in cell ablated retina. (A) TH$^+$ cells in regenerated retina (red cells) to the right of the image, as well as 5HT$^+$ cells (green cells, arrows). The dotted line estimates the boundary between extant (left) and regenerated retina (right). Note the absence of TH$^+$ cells, and presence of 5-HT$^+$ cells, in the 6-OHDA-exposed region of retina (to the left of the dotted line). (B) Normalized cell densities as a function of distance from the edge of the lesion site. TH$^+$ cell density (red) was significantly elevated in regenerated region within the first 50 μm of growth adjacent to the neurotoxin exposed retina (*, $p < .05$). 5-HT$^+$ cell density (green) was not significantly affected (see Section 3).

lesion edge (Fig. 3B; $p < .05$). This region of elevated density corresponds to retina regenerated immediately subsequent to injury (Hitchcock et al., 1992), and its presence $\geqslant 12$ weeks post-lesion was consistent with a lack of significant "pruning" by cell death or lateral migration. There was no corresponding elevation in the density of 5-HT$^+$ cells (Fig. 3B). This regional, cell-type-specific hyperplasia was conceptually identical to that observed for normal retinal growth following neurotoxin exposure (Tyler et al., 2005), and the operation of similar patterning mechanisms during retinal regeneration was thus indicated.

3.3. Computational modeling of pattern formation in regenerated retina

Because the spatiotemporal control of cell fate acquisition, and not cell death or cell migration, evidently domi-

nates the formation of TH$^+$ cellular patterns in the growing goldfish retina, the contribution of this mechanism to the regeneration of TH$^+$ patterns was assessed using a computational model (see Section 3). Fields of model-derived control retina (Fig. 4A) contained patterns of TH$^+$ cells that were not statistically different from the *in vivo* control patterns, as determined by NND, DRP (i.e., effective radius), and quadrat analyses (Table 2). Patches of defined geometries were removed to simulate retinal lesions (Fig. 4B–D). These model-derived regenerated patterns were produced with the same model parameter values as used for TH$^+$ cell production during normal retinal growth (Tyler et al., 2005). The model-derived regenerated patterns were statistically compared to the model-derived control patterns, with summary information for each data set provided in Table 2.

For all lesion geometries (circular, square, and jagged) model-derived regenerated cellular patterns had aNND distributions that were greater (Fig. 5A), CR values that were significantly lower (Fig. 5B), effective radius values that were greater (Fig. 5C, with the exception of the jagged patterns), and densities that were significantly smaller (Fig. 5D) than the model-derived control patterns. Compared to control patterns, quadrat analysis revealed that regenerated patterns also tended to be less regular (Table 2). The geometry of the surgical lesions apparently influenced the ability of the model to simulate regenerated cellular patterns, with the jagged lesion simulations producing patterns that were most similar to those observed *in vivo*. These analyses indicated that although the model-derived regenerated patterns tended to
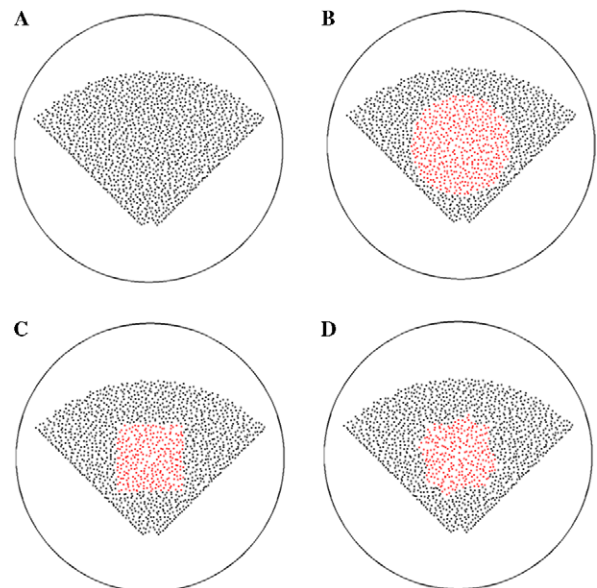

Fig. 4. Model-derived patterns of TH$^+$ cells in control and regenerated retina. (A) The fan-shaped distribution of black circles denotes the positions of model-generated TH$^+$ cells in a "control" retina. With the expected exception of conformity ratio, spatial analyses revealed no significant difference between the model-derived and *in vivo* control patterns of TH$^+$ cells (see Table 2). Examples of circular (B), square (C), or jagged (D) excisions from the control pattern of (A) are illustrated, within which model-derived, regenerated patterns of TH$^+$ cells were produced (red).

Table 2
Spatial analyses of model-derived control and regenerated patterns of TH$^+$ cells

ID (n)	NND (µm) Mean±SD	CR	Density (mm^{-2})	R$_{eff}$ (µm)	Quadrat
Control					
TH1a (39)	85.2±19.6	4.3	77.4	70	Regular
TH1b (56)	74.2±14.7	5.0	111.1	62	Regular
TH2a (36)	85.1±19.3	4.4	71.4	65	Regular
TH2b (44)	76.6±18.3	4.2	87.3	65	Regular
TH3a (34)	96.6±12.8	7.5	67.5	75	Regular
TH3b (35)	88.2±16.9	5.2	69.4	86	Regular
TH4a (35)	91.0±20.5	4.4	69.4	88	Regular
TH4b (28)	103.1±12.9	8.0	55.6	84	Regular
TH5a (33)	90.7±16.0	5.7	65.5	79	Regular
TH5b (26)	96.8±21.3	4.5	51.6	71	Regular
TH6a (34)	92.5±18.7	4.9	67.5	75	Regular
TH6b (37)	89.2±17.2	5.2	73.4	73	Regular
Mean±SD	**89.1±8.2**	5.3±1.2	72.3±15.3	**74.4±8.5**	
In vivo test (p)	.37	<.01	.45	.66	
Circular lesion					
TH1a (36)	90.8±19.7	4.6	71.4	66	Regular
TH1b (46)	74.3±19.7	3.8	91.3	61	Regular
TH2a (31)	90.1±25.1	3.6	61.5	82	Regular
TH2b (36)	88.2±22.6	3.9	71.4	76	Regular
TH3a (26)	108.5±18.0	6.0	51.6	87	Regular
TH3b (27)	97.5±26.3	3.7	53.6	84	Reg/rand
TH4a (25)	99.5±26.1*	3.8	49.6	92	Reg/rand
TH4b (22)	121.1±36.8	3.3	43.7	103	Regular
TH5a (26)	102.2±20.6	5.0	51.6	93	Reg/rand
TH5b (24)	110.5±29.4	3.8	47.6	95	Reg/rand
TH6a (25)	99.8±26.1	3.8	49.6	85	Reg/rand
TH6b (30)	99.8±28.9	3.5	59.5	73	Regular
Mean±SD	98.5±12.0	4.1±0.8	58.5±13.6	83.1±12.3	
In vivo test (p)	<.001	<.001	<.001	<.001	
Square lesion					
TH1a (33)	96.1±18.8	5.1	65.5	77	Regular
TH1b (49)	76.6±16.2	4.7	97.2	61	Regular
TH2a (32)	94.7±22.0	4.3	63.5	79	Regular
TH2b (42)	85.6±21.2	4.0	83.3	71	Regular
TH3a (26)	96.0±30.7	3.1	51.6	79	Reg/rand
TH3b (28)	91.7±24.9	3.7	55.6	77	Reg/rand
TH4a (27)	107.1±28.5	3.8	53.6	93	Reg/rand
TH4b (22)	116.5±37.4	3.1	43.7	83	Reg/rand
TH5a (27)	102.7±26.3	3.9	53.6	91	Reg/rand
TH5b (22)	119.4±28.9	4.1	43.7	100	Regular
TH6a (26)	103.7±28.0	3.7	51.6	86	Reg/rand
TH6b (29)	85.9±29.2	2.9	57.5	50	Reg/rand
Mean±SD	98.0±12.6	3.9±0.6	60.0±15.8	78.9±13.8	
In vivo test (p)	<.001	<.001	<.001	<.001	
Jagged lesion					
TH1a (36)	78.1±23.5	3.3	71.4	68	Regular
TH1b (47)	73.8±17.5	4.2	93.3	48	Regular
TH2a (32)	83.1±18.6	4.5	63.5	50	Regular
TH2b (39)	80.6±25.1	3.2	77.4	65	Reg/rand
TH3a (28)	90.4±39.1	2.3	55.6	0	Random
TH3b (29)	86.9±30.9	2.8	57.5	50	Random
TH4a (29)	92.4±23.0	4.0	57.5	78	Regular
TH4b (25)	101.1±34.7	2.9	49.6	82	Random
TH5a (28)	98.7±28.4	3.5	55.6	75	Reg/rand
TH5b (19)	110.4±34.7	2.9	37.7	79	Reg/rand
TH6a (29)	91.9±32.1	3.5	57.5	52	Reg/rand
TH6b (32)	98.6±28.1	3.2	63.5	77	Regular
Mean±SD	90.5±10.6	3.4±0.6	61.7±14.1	**60.3±22.9**	
In vivo test (p)	<.001	<.01	<.001	.11	

For each category the spatial analyses are statistically compared to the corresponding *in vivo* control or regenerated data set (Table 1), with attendant *p* values indicated for independent *t*-test analysis. Summary values in bold font are not significantly different from the corresponding *in vivo* data. The circular, square, and jagged data sets correspond to the geometry of the modeled lesion site (Fig. 4). Terminologies as in Table 1.
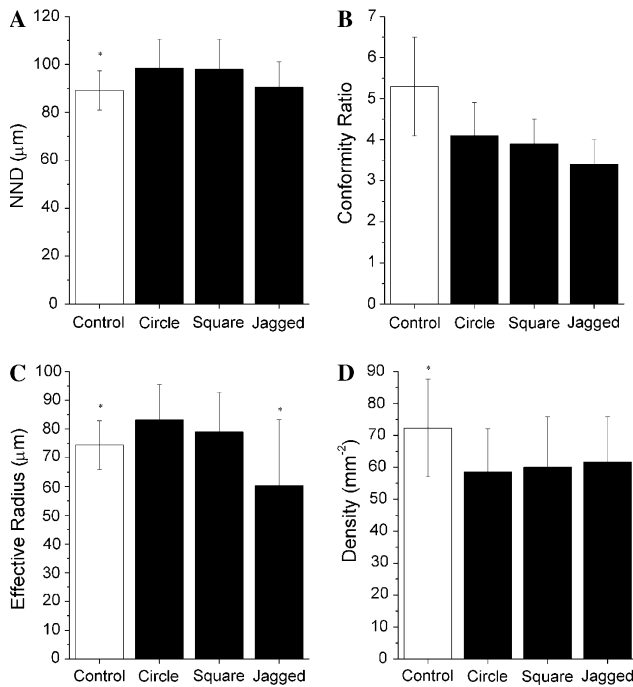
Fig. 5. Spatial analysis of model-derived control and regenerated TH[+] cell patterns. In all plots mean ± standard deviation are indicated for control (open bars) and regenerated patterns (filled bars), the latter including circular, square, and jagged lesion geometries. NND (A), conformity ratio (B), effective radius (C), and density (D) analyses are plotted as in Fig. 2. Asterisks indicate distributions not significantly different ($p > .05$) from the corresponding *in vivo* control or regenerated patterns (see Table 2).

Cameron & Carney, 2004). Adjustment was made to minimize the error in mean cell density between the *in vivo* regenerated cell patterns and the model jagged edged regenerated cells patterns (cf. Tables 1 and 3). At the level of undifferentiated progenitors this adjustment is consistent with either a decrease in the amount or level of the receptor/detector mechanism for the signal that inhibits cell fate acquisition, or diminished signaling efficacy through the underlying transduction pathway; as with our simulations of normal retinal growth (Tyler et al., 2005), increases in modeled progenitor cell density did not significantly affect the regenerated cell patterns (data not shown).

By decreasing the threshold parameter representing undifferentiated cells' sensitivity to the inhibitory signal from -1.0 to -1.8 ± 0.7 ($n = 12$), but changing no other simulation parameters, model-derived regenerated patterns were produced with aNND, DRP, and density results insignificantly different from those of *in vivo* regenerated retina (Table 3; Fig. 6A, C, and D). Like simulations of control retinal growth the modeled CR values of regenerated retina were consistently greater than the *in vivo* patterns (Cameron & Carney, 2004; Tyler et al., 2005), indicating that although a certain degree of 'noise' in the biological patterning mechanism is absent from the model, the model still produces good pattern estimates over short and long spatial scales (cf. Tables 1 and 3, Figs. 2B, 6B). These results indicate that although a general negative feedback scheme for regulating cell fate acquisition can account for the formation of cellular patterns during both normal retinal growth and regeneration, some fundamental aspect of the signaling scheme must be different between the two cytogenic conditions.

4. Discussion

A computational model that successfully simulates pattern formation of inner retinal cells in the growing goldfish

be significantly different from the control patterns, with the jagged lesion geometry best matching the empirical data, they were in general poor estimates of the *in vivo* regenerated patterns (cf. Tables 1 and 2).

In an effort to improve the simulations of regenerative pattern formation, a single model parameter that controls the undifferentiated cells' sensitivity (i.e., threshold) to the feedback inhibitory signal was adjusted (see Fig. 8 of

Table 3
Spatial analyses of adjusted model-derived patterns of regenerated TH^{+} cells

ID (n)	Threshold	NND (µm) mean ± SD	CR	Density (mm^{-2})	Reff (µm)	Quadrat
Adjusted jagged regenerated						
TH1a (48)	−1.5	74.6 ± 21.9	3.4	95.2	62	Regular
TH1b (47)	−1.01	78.8 ± 18.6	4.2	93.3	50	Regular
TH2a (49)	−1.7	69.4 ± 23.3	3.0	97.2	46	Regular
TH2b (45)	−1.2	68.6 ± 19.8	3.5	89.3	49	Regular
TH3a (48)	−1.75	59.0 ± 15.1	3.9	95.2	34	Reg/rand
TH3b (55)	−2.1	69.6 ± 23.0	3.0	109.1	74	Regular
TH4a (49)	−2.1	66.6 ± 17.1	3.9	97.2	41	Regular
TH4b (60)	−3.1	60.6 ± 20.5	3.0	119.0	42	Regular
TH5a (31)	−1.1	86.5 ± 26.3	3.3	61.5	50	Regular
TH5b (59)	−3.1	55.0 ± 26.7	2.1	117.1	53	Reg/rand
TH6a (43)	−1.75	69.4 ± 26.6	2.6	85.3	49	Regular
TH6b (43)	−1.5	70.0 ± 17.6	4.0	85.3	66	Regular
Mean ± SD	−1.8 ± 0.7	**69.0 ± 8.6**	3.3 ± 0.6	**95.4 ± 15.4**	**51.3 ± 11.2**	
In vivo test (p)		.31	<.01	.99	.34	

The jagged lesion geometry was used for all simulations. For each simulation ID (matching that of the jagged data set in Table 2), the model parameter representing threshold for the inhibitory signal (Cameron & Carney, 2004) was adjusted downward to achieve a match between the model-derived and *in vivo* regenerated density of cells (see Section 3). Symbols, terminology, and statistical comparisons are the same as those of Table 2.
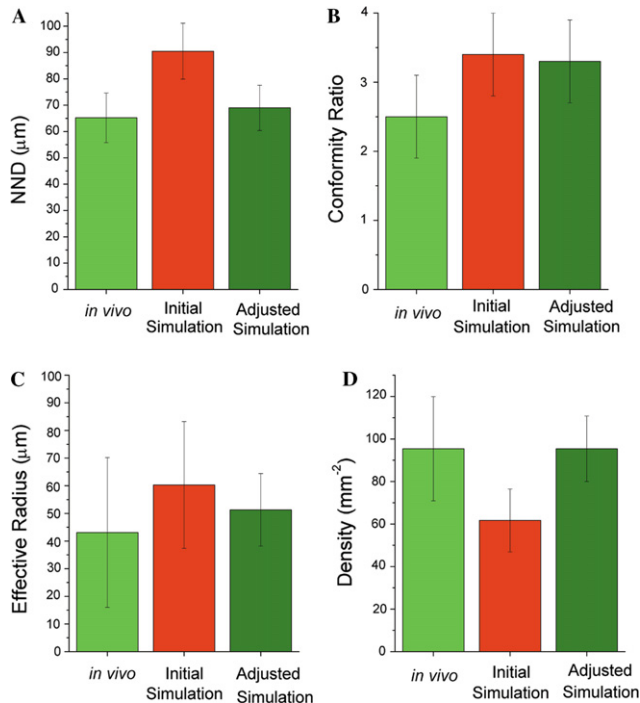
Fig. 6. Spatial analysis of adjusted model-derived regenerated TH$^+$ cell patterns. Mean ± standard deviation for NND (A), conformity ratio (B), effective radius (C), and density (D) analyses are plotted for *in vivo* regenerated TH$^+$ patterns (light green bars), initial model simulations of jagged geometry regenerated patterns (red bars), and adjusted model simulations with lowered threshold (dark green bars; see Section 3). With the exception of conformity ratio the adjusted model patterns are not significantly different from *in vivo* regenerated patterns (Tables 1 & 3).

retina is shown here to also reproduce quantitative features of cellular patterns in regenerated retina. These successful simulations suggest that pattern formation during retinal regeneration recapitulates that of normal retinal growth, and involves the operation of negative feedback signals through which differentiated cells regulate the acquisition of homotypic cell fates by undifferentiated progenitors. The modeling results also predict specific differences between normal and regenerative retinal progenitors.

4.1. Retinal regeneration – outcomes and hypothesized mechanisms

Quantitative analysis of regenerated patterns of TH$^+$ cells in the goldfish retina revealed consistent differences with their control counterparts. These differences include an elevated density and an overall less regular distribution across two-dimensional space, similar to patterning attributes reported previously for several cell types (Cameron & Carney, 2000; Cameron & Easter, 1995; Hitchcock & Van-DeRyt, 1994). Because cellular patterning directly affects functionality, defects in patterning could impose deficits upon retinal function, including the retina's ability to process spatial and spectral aspects of the visual scene (Cameron, Cornwall, & MacNichol, 1997; Cameron & Powers, 2000). That neurons are regenerated at all, however, and in

non-random patterns reminiscent of control retina, suggests the restoration of a physical substrate that can accommodate substantial functional recovery, as suggested from physiological investigations (Chiba et al., 2004; Mensinger & Powers, 1999; Ohmasa & Saito, 2004).

Cell ablation experiments confirmed a dominant role for spatial control of cell fate acquisition in the patterning of regenerated retina. Specifically, the persistent, regional, cell-type-specific elevated density of the ablated cell type near the original lesion boundary (Fig. 3) was consistent with a lack of significant cell migration or death. The operation of either mechanism should have ultimately resolved the hyperplasia; e.g., by migration of cells into the adjoining neurotoxin exposed retina. The persistence of atypical regenerated patterns *in vivo* also argues against pattern 'pruning' by cell death or migration. As with normal retinal growth, a dominant role for cell-type-defining, fate-promoting signals during regeneration was ruled out by the anti-clustered characteristic of the regenerated patterns and the lack of evidence for positive correlation between the patterns of different cell types (Cameron & Carney, 2004). The regional, cell-type-specific hyperplasia is, however, consistent with the transient removal of a signal that inhibits, in a cell-type-specific manner, cell fate acquisition. The reacquisition of this signal as the retina regenerates (i.e., as new TH$^+$ cells are produced) is hypothesized to limit the spatial extent of the regional elevated density. This inference of a specific patterning mechanism is similar to that reported previously for retinal growth in this system (Tyler et al., 2005), and suggests that regenerating adult retina has access to, and utilizes, the same patterning mechanisms as in operation during normal retinal growth.

4.2. A hypothesized molecular basis for atypical cellular patterns in regenerated retina

As an initial step toward understanding the physical determinants of the atypical cellular patterns of regenerated retina, simulations of retinal regeneration were performed using different lesion geometries. All simulations utilized the same cell-type-specific, negative feedback signals originating from differentiated cells as inferred for normal retinal growth. Regardless of the specific lesion geometry the simulated regenerated patterns displayed spatial attributes significantly different from control retina. It is hypothesized that the multiple directions of regenerating growth into the lesion site sets up a complex 'wave front' of inhibitory signaling that differs from that of normal growth (see Fig. 1 of Cameron & Carney, 2004) and produces an atypical spatial distribution of cell fate acquisition.

When using model parameters appropriate for normal growth (Tyler et al., 2005), the model reproduced qualitative aspects of regenerated patterns, but failed to recapitulate quantitative aspects of the regenerated patterns, regardless of lesion geometry (Table 2, Fig. 7A). Simulated regenerated patterns that statistically matched those of *in vivo* regenerated retina could be reliably produced,

however, by adjusting a single parameter of the model. This parameter represents the sensitivity of progenitors to the inhibitory signal regulating cell fate acquisition, or equivalently reducing the amount of signal present. The model does not differentiate between these two effects, but the former was chosen for adjustment because of the lack of any explicit evidence to suggest that differentiated cells surrounding the lesion site differ from their counterparts at the retinal margin. By adjusting the sensitivity parameter downward, simulated regenerated patterns that matched the *in vivo* patterns were consistently produced (Table 3; Fig 7B and C). No other model parameter needed to be adjusted, including the space constant of the inferred inhibitory signal (Cameron & Carney, 2004) or the density of progenitor cells (Tyler et al., 2005), suggesting that the same molecular signal(s) could mediate patterning during regeneration and normal growth. Although not formally exclusionary, the cell ablation experiments also argued against the hypothesis that set of signals different from those affecting normal retinal growth are in operation during regeneration (see below). These results supported the hypothesis that cellular patterning during regeneration involves the recapitulation of developmental mechanisms that regulate cell fate acquisition.

The mechanisms that enable an adult retina to regenerate are not well defined, but are likely to involve a complex set of cellular and transcriptional events (Cameron et al., 2005). At the cellular level recent investigations indicate that Müller cells can exhibit a regenerative 'stem cell' phenotype following retinal damage (Fausett & Goldman, 2006; Fischer & Reh, 2001, 2003; Garcia & Vecino, 2003; Wu et al., 2001; Yurco & Cameron, 2005). Whether these injury induced stem cells are functionally identical to those associated with normal retinal growth is unknown, but our modeling results suggest they are not. Specifically, to successfully simulate regenerated cellular patterns, progenitors with significantly lower sensitivity to the signals that inhibit cell fate acquisition were required. This result predicts that, compared to their counterparts at the circumferential germinal zone (CGZ), regenerative progenitors in this system manifest lower expression/production of the receptor, and/or a less effective transduction pathway, leading to the cell fate decision mechanism. Such a dichotomy may not be surprising given the different cellular histories of the growth and regenerative progenitor cells. Unlike regenerative progenitors, cells at the CGZ are likely to not arise from Müller cells (or any other differentiated retinal cell type), and instead are likely a self-renewing population with origins early in development. That distinct populations of intrinsic progenitors could produce the full complement of differentiated retinal cells might ultimately have implications regarding the development of strategies based upon stem cells for effecting cellular repair in damaged or diseased retina. It remains possible that physical parameters of the inhibitory feedback mechanism might vary between normal and regenerated retina: differences in the microenvironment might affect signal diffusion, and newly regenerated cells might produce less of the signal. Because the empirical foundations of these (and other) possibilities is quite limited, for the current study we chose to manipulate the threshold parameter, from which explicit and testable predictions arise; i.e., that regenerative precursors might express less receptor than their counterparts at the CGZ.

4.3. Candidate pattern formation signals

Cellular pattern formation in the CNS is a highly complex phenomenon, involving the coordinated production of millions of cells via signaling mechanisms involving direct contact (Austin, Feldman, Ida, & Cepko, 1995; Spana & Doe, 1996; Umino & Saito, 2002) and diffusible molecules (Hyatt, Schmitt, Fadool, & Dowling, 1996; Neumann & Nuesslein-Volhard, 2000; Strutt & Strutt, 2003; Waid & McLoon, 1998). Furthermore, the mechanisms affecting cell fate acquisition within the CNS appear to be location-specific (Chizhikov & Millen, 2005; Wilson & Maden, 2005) and even time-specific (Binor & Heathcote, 2005). Computational modeling presents an opportunity to simplify the investigation of this complex topic by generating testable predictions about a restricted, well-defined set of hypothetical patterning mechanisms. Although an infinite number of disparate patterning mechanisms could, in theory, account for the observed cellular patterns, our relatively simple "one step" model of cell fate acquisition in the retina is parsimonious and explains inner retinal pattern formation during both growth and regeneration.

Previous investigations have revealed the operation of inhibitory signaling molecules that affect phenotypic assignments in the retina (Belliveau & Cepko, 1999; Negishi et al., 1982, 1985; Reh & Tully, 1986; Waid & McLoon, 1998). The results from our present and previous studies (Cameron & Carney, 2000, 2004; Tyler et al., 2005) define at least three constraints that must be met by any candidate signaling mechanism controlling cell fate acquisition in this system: (1) it must be present during both normal growth and regeneration; (2) it must control cell fate acquisition in an inhibitory, cell-type-specific manner; (3) the spatiotemporal attributes of the signaling mechanisms, and thus their molecular components (receptors, ligands, etc.) are invariant between growth and regeneration.

We hypothesize that neurotransmitters could meet the above criteria and could thus function as agents that inhibit the acquisition of specific cell fates during retinal growth and regeneration. This hypothesis does not rule out the operation of other agents (e.g., neurotrophins) in cellular patterning, nor does it preclude distinct cell types from sharing a common patterning signal. Neurotransmitters are present, however, during both normal and regenerative growth, are selectively produced by differentiated retinal cells, and could influence cellular phenomena over relatively large distances. Furthermore, both dopamine and serotonin have been shown to affect various aspects of

neuronal development (e.g., Buznikov, Shmukler, & Lauder, 1999; Herlenius & Lagercrantz, 2001; Lankford, DeMello, & Klein, 1998; Lima & Schmeer, 1994; Lima, Urbina, Matus, & Drujan, 1996; Moiseiwitsch, 2000; Rodrigues & Dowling, 1990; Zachor, Moore, Brezausek, Theibert, & Percy, 2000). These findings provide indirect support for the role of neurotransmitters as feedback modulators of cell fate acquisition in the retina, and experiments designed to directly test this hypothesis are currently being pursued.

Acknowledgments

References

Austin, C. P., Feldman, D. E., Ida, J. A., Jr., & Cepko, C. L. (1995). Vertebrate retinal ganglion cells are selected from competent progenitors by the action of Notch. *Development, 121*, 3637–3650.

Belliveau, M. J., & Cepko, C. L. (1999). Extrinsic and intrinsic factors control the genesis of amacrine and cone cells in the rat retina. *Development, 126*, 555–566.

Binor, E., & Heathcote, R. D. (2005). Activated notch disrupts the initial patterning of dopaminergic spinal cord neurons. *Developmental Neuroscience, 27*, 306–312.

Braisted, J. E., Essman, T. F., & Raymond, P. A. (1994). Selective regeneration of photoreceptors in goldfish retina. *Development, 120*, 2409–2419.

Buznikov, G. A., Shmukler, Y., & Lauder, J. M. (1999). Changes in the physiological roles of neurotransmitters during individual development. *Neuroscience and Behavioral Physiology, 29*, 11–21.

Cameron, D. A., & Carney, L. H. (2000). Cell mosaic patterns in the native and regenerated inner retina of zebrafish: implications for retinal assembly. *Journal of Comparative Neurology, 416*, 356–367.

Cameron, D. A., & Carney, L. H. (2004). Cellular patterns in the inner retina of adult zebrafish: Quantitative analyses and a computational model of their formation. *Journal of Comparative Neurology, 471*, 11–25.

Cameron, D. A., Cornwall, M. C., & MacNichol, E. F., Jr. (1997). Visual pigment assignments in regenerated retina. *Journal of Neuroscience, 17*, 917–923.

Cameron, D. A., & Easter, S. S., Jr. (1995). Cone photoreceptor regeneration in adult fish retina: Phenotypic determination and mosaic pattern formation. *Journal of Neuroscience, 15*, 2255–2271.

Cameron, D. A., Gentile, K. L., Middleton, F. A., & Yurco, P. (2005). Gene expression profiles of intact and regenerating zebrafish retina. *Molecular Vision, 11*, 775–791.

Cameron, D. A., & Powers, M. K. (2000). Morphology and visual pigment content of photoreceptors from injured goldfish retina. *Visual Neuroscience, 17*, 623–630.

Cheon, E. W., Kuwata, O., & Saito, T. (2001). Muscarinic acetylcholine receptors in the normal, developing and regenerating newt retinas. *Brain Research Developmental Brain Research, 127*, 9–21.

Chiba, C., Nakamura, K., Unno, S., & Saito, T. (2004). Intraocular implantation of DNA-transfected retinal pigment epithelium cells: A new approach for analyzing molecular functions in the newt retinal regeneration. *Neuroscience Letters, 368*, 171–175.

Chiba, C., Oi, H., & Saito, T. (2005). Changes in somatic sodium currents of ganglion cells during retinal regeneration in the adult newt. *Brain Research Developmental Brain Research, 154*, 25–34.

Chizhikov, V. V., & Millen, K. J. (2005). Roof plate-dependent patterning of the vertebrate dorsal central nervous system. *Developmental Biology, 277*, 287–295.

Cook, J. E. (1996). Spatial properties of retinal mosaics: An empirical evaluation of some existing measures. *Visual Neuroscience, 13*, 15–30.

Eglen, S. J., van Ooyen, A., & Willshaw, D. J. (2000). Lateral cell movement driven by dendritic interactions is sufficient to form retinal mosaics. *Network Computation in Neural Systems, 11*, 103–118.

Eglen, S. J., & Willshaw, D. J. (2002). Influence of cell fate mechanisms upon retinal mosaic formation: A modelling study. *Development, 129*, 5399–5408.

Fausett, B. V., & Goldman, D. (2006). A role for alpha1 tubulin-expressing Müller glia in regeneration of the injured zebrafish retina. *Journal of Neuroscience, 26*, 6303–6313.

Fischer, A. J., & Reh, T. A. (2001). Müller glia are a potential source of neural regeneration in the postnatal chicken retina. *Nature Neuroscience, 4*, 247–252.

Fischer, A. J., & Reh, T. A. (2003). Potential of Müller glia to become neurogenic progenitor cells. *Glia, 43*, 70–76.

Garcia, M., & Vecino, E. (2003). Role of Müller glia in neuroprotection and regeneration in the retina. *Histology and Histopathology, 18*, 1205–1218.

Goldman, D., Hankin, M., Li, Z., Dai, X., & Ding, J. (2001). Transgenic zebrafish for studying nervous system development and regeneration. *Transgenic Research, 10*, 21–33.

Greig-Smith, P. (1957). *Quantitative plant ecology*. London: Butterworths.

Herlenius, E., & Lagercrantz, H. (2001). Neurotransmitters and neuromodulators during early human development. *Early Human Development, 65*, 21–37.

Hitchcock, P. F., Lindsey Myhr, K. J., Easter, S. S., Jr., Mangione-Smith, R., & Jones, D. D. (1992). Local regeneration in the retina of the goldfish. *Journal of Neurobiology, 23*, 187–203.

Hitchcock, P. F., & VanDeRyt, J. T. (1994). Regeneration of the dopamine-cell mosaic in the retina of the goldfish. *Visual Neuroscience, 11*, 209–217.

Hyatt, G. A., Schmitt, E. A., Fadool, J. M., & Dowling, J. E. (1996). Retinoic acid alters photoreceptor development in vivo. *Proceedings of the National Academy of Sciences USA, 93*, 13298–13303.

Lankford, K. L., DeMello, F. G., & Klein, W. L. (1988). D$_1$-type dopamine receptors inhibit growth cone motility in cultured retina neurons: Evidence that neurotransmitters act as morphogenetic growth regulators in the developing central nervous system. *Proceedings of the National Academy of Sciences USA, 85*, 2839–2843.

Lima, L., & Schmeer, C. (1994). Characterization of serotonin transporter in goldfish retina by the binding of [^{3}H]paroxetine and the uptake of [^{3}H]serotonin: Modulation by light. *Journal of Neurochemistry, 62*, 528–535.

Lima, L., Urbina, M., Matus, P., & Drujan, Y. (1996). Synthesis of serotonin from 5-hydroxytryptophan in the post-crush retina: Inhibition of in vitro outgrowth by the intraocular administration of the precursor. *Neurochemical Research, 21*, 939–946.

Mader, M. M., & Cameron, D. A. (2004). Photoreceptor differentiation during retinal development, growth, and regeneration in a metamorphic vertebrate. *Journal of Neuroscience, 24*, 11463–11472.

Mensinger, A. F., & Powers, M. K. (1999). Visual function in regenerating teleost retina following cytotoxic lesioning. *Visual Neuroscience, 16*, 241–251.

Moiseiwitsch, J. R. (2000). The role of serotonin and neurotransmitters during craniofacial development. *Critical Reviews in Oral Biology and Medicine, 11*, 230–239.

Naruoka, H., Kojima, R., Ohmasa, M., Layer, P. G., & Saito, T. (2003). Transient muscarinic calcium mobilisation in transdifferentiating as in reaggregating embryonic chick retinae. *Brain Research Developmental Brain Research, 143*, 233–244.

Negishi, K., Teranishi, T., & Kato, S. (1982). New dopaminergic and indoleamine-accumulating cells in the growth zone of goldfish retinas after neurotoxic destruction. *Science, 216*, 747–749.

Negishi, K., Teranishi, T., & Kato, S. (1985). Growth rate of a peripheral annulus defined by neurotoxic destruction in the goldfish retina. *Brain Research, 352*, 291–295.

Neumann, C. J., & Nuesslein-Volhard, C. (2000). Patterning of the zebrafish retina by a wave of sonic hedgehog activity. *Science, 289*, 2137–2139.

Ohmasa, M., & Saito, T. (2004). GABAA-receptor-mediated increase in intracellular Ca^{2+} concentration in the regenerating retina of adult newt. *Neuroscience Research, 49*, 219–227.

Otteson, D. C., & Hitchcock, P. F. (2003). Stem cells in the teleost retina: Persistent neurogenesis and injury-induced regeneration. *Vision Research, 43*, 927–936.

Raven, M. A., Eglen, S. J., Ohab, J. J., & Reese, B. E. (2003). Determinants of the exclusion zone in dopaminergic amacrine cell mosaics. *Journal of Comparative Neurology, 461*, 123–136.

Raymond, P. A., & Hitchcock, P. F. (2000). How the neural retina regenerates. *Results and Problems in Cell Differentiation, 31*, 197–218.

Reh, T. A., & Levine, E. M. (1998). Multipotential stem cells and progenitors in the vertebrate retina. *Journal of Neurobiology, 36*, 206–220.

Reh, T. A., & Tully, T. (1986). Regulation of tyrosine hydroxylase-containing amacrine cell number in larval frog retina. *Developmental Biology, 114*, 463–469.

Rodieck, R. W. (1991). The density recovery profile: a method for the analysis of points in the plane applicable to retinal studies. *Visual Neuroscience, 6*, 95–111.

Rodrigues, S., & Dowling, J. E. (1990). Dopamine induces neurite retraction in retinal horizontal cells via diacylglycerol and protein kinase C. *Proceedings of the National Academy of Sciences USA, 87*, 9693–9697.

Saito, T., Kaneko, Y., Maruo, F., Niino, M., & Sakaki, Y. (1994). Study of the regenerating newt retina by electrophysiology and immunohistochemistry (bipolar- and cone-specific antigen localization). *Journal of Experimental Zoology, 270*, 491–500.

Spana, E. P., & Doe, C. Q. (1996). Numb antagonizes Notch signaling to specify sibling neuron cell fate. *Neuron, 17*, 21–26.

Stenkamp, D. L., & Cameron, D. A. (2002). Cellular pattern formation in the retina: Retinal regeneration as a model system. *Molecular Vision, 8*, 280–293.

Stenkamp, D. L., Powers, M. K., Carney, L. H., & Cameron, D. A. (2001). Evidence for two distinct mechanisms of neurogenesis and cellular pattern formation in regenerated goldfish retinas. *Journal of Comparative Neurology, 431*, 363–381.

Strutt, H., & Strutt, D. (2003). EGF signaling and ommatidial rotation in the *Drosophila* eye. *Current Biology, 13*, 1451–1457.

Tohya, S., Mochizuki, A., & Iwasa, Y. (1999). Formation of cone mosaic of zebrafish retina. *Journal of Theoretical Biology, 200*, 231–244.

Tohya, S., Mochizuki, A., & Iwasa, Y. (2003). Difference in the retinal cone mosaic pattern between zebrafish and medaka: Cell-rearrangement model. *Journal of Theoretical Biology, 221*, 289–300.

Tyler, M., Carney, L. H., & Cameron, D. A. (2005). Control of cellular pattern formation in the vertebrate retina by homotypic regulation of cell fate decisions. *Journal of Neuroscience, 25*, 4565–4576.

Umino, Y., & Saito, T. (2002). Spatial and temporal patterns of distribution of the gap junctional protein connexin43 during retinal regeneration of adult newt. *Journal of Comparative Neurology, 454*, 255–262.

Waid, D. K., & McLoon, S. C. (1998). Ganglion cells influence the fate of dividing retinal cells in culture. *Development, 125*, 1059–1066.

Watling, K. J., Parkinson, D., & Dowling, J. E. (1982). Effects of intraocular injections of 6-hydroxydopamine on dopamine-dependent cyclic AMP accumulation in intact pieces of carp retina. *Brain Research, 253*, 334–336.

Wilson, L., & Maden, M. (2005). The mechanisms of dorsoventral patterning in the vertebrate neural tube. *Developmental Biology, 282*, 1–13.

Wu, D. M., Schneiderman, T., Burgett, J., Gokhale, P., Barthel, L., & Raymond, P. A. (2001). Cones regenerate from retinal stem cells sequestered in the inner nuclear layer of adult goldfish retina. *Investigative Ophthalmology and Visual Science, 42*, 2115–2124.

Yazulla, S., & Studholme, K. M. (1997). Differential reinnervation of retinal bipolar cell dendrites and axon terminals by dopamine interplexiform cells following dopamine depletion with 6-OHDA. *Journal of Comparative Neurology, 382*, 535–545.

Yurco, P., & Cameron, D. A. (2005). Responses of Müller glia to retinal injury in adult zebrafish. *Vision Research, 45*, 991–1002.

Zachor, D. A., Moore, J. F., Brezausek, C., Theibert, A., & Percy, A. K. (2000). Cocaine inhibits NGF-induced PC12 cells differentiation through D_1-type dopamine receptors. *Brain Research, 869*, 85–97.